A Polycyclic Aromatic Hydrocarbon Containing A Pyrrolopyridazine Core

Marcus Richter,[a] Yubin Fu,[a] Evgenia Dmitrieva,[b] Jan J. Weigand,[c] Alexey Popov,[b] Reinhard Berger,[a] Junzhi Liu,[a] Xinliang Feng*[a]

Abstract: Polycyclic aromatic azomethine ylide (PAMY) is a versatile building block for the bottom-up construction of unprecedented nitrogen-containing polycyclic aromatic hydrocarbons (N-PAHs). Here, we demonstrate the 1,3-dipolar cycloaddition between PAMY and 1,4-diphenylbut-2-yne-1,4-dione as well as the subsequent condensation reaction with hydrazine, which led to synthesis of unique N-PAHs with a phenyl-substituted pyrrolopyridazine core (**PP-1** and **PP-2**). The molecular structures of pristine **PP-1** and *tert*-butyl-substituted **PP-2** were verified by NMR and mass spectroscopy. Moreover, the structure of **PP-2** was unambiguously elucidated by X-ray single crystal analysis. The optoelectronic properties were investigated by solvent-dependent UV-Vis absorption and fluorescence emission spectroscopy as well as cyclic voltammetry. Additionally, the density functional theory (DFT) calculations exhibited a push-pull behavior for **PP-1** and **PP-2**. Furthermore, the *in situ* EPR/UV-Vis-NIR spectroelectrochemistry allowed the detailed insight into the spectroscopic properties and spin distribution of radical cation species of **PP-2**.

Due to their potential applications in nano- and optoelectronics, the interest in polycyclic aromatic hydrocarbons (PAHs) has increased throughout the last two decades.[1] However, the electronic structure and optical properties of PAHs highly depend on their size, geometry and periphery substitution.[2] The introduction of heteroatoms, like nitrogen, into the sp^2-hybridized polycyclic aromatic framework is a further effective strategy to tailor their intrinsic physical and chemical properties, such as decreasing the lowest unoccupied molecular orbital (LUMO) level, rendering binding sites to metal atoms, or stabilizing oxidized as well as reduced species.[3] In particular, the amount and the precise position of the nitrogen atom significantly influence the electronic features of nitrogen-containing PAHs (N-PAHs, Figure 1). For example, the introduction of nitrogen atoms into the periphery, like in azapentacene **I** or tetraazaperylene derivate **II**, offers electron-deficient N-PAHs.[4] In contrast, the internal implementation of nitrogen atoms into the pristine carbon framework via a pyrrole ring, such as in pyrrole-fused azacoronene **III** or hydrazine-embedded buckybowl **IV**, leads to electron-rich N-PAHs.[5] Nevertheless, it remains challenging to incorporate nitrogen atoms selectively and precisely in the basal plane of PAHs.[6]

One attractive building block for the synthesis of novel N-PAHs is the polycyclic aromatic azomethine ylide (PAMY), which was first developed by our group.[7] Besides the dimerization of PAMYs to pyrazine-embedded PAHs at high temperatures, the zwitterionic character enables the 1,3-dipolar cycloaddition at room temperature, which serves as an efficient strategy for the synthesis of pyrrole-incorporated PAHs.[7-8] Recently, our group, as well as Ito´s group, extended the range of dipolarophiles and reported on the cycloaddition of PAMYs with asymmetric or pristine carbon dipolarophiles, such as 1,2-naphthoquinone and coronene, respectively.[9]

Herein, we present the synthesis of unprecedented N-PAHs containing a diphenyl-substituted pyrrolopyridazine core (**PP-1** and **PP-2**) via cycloaddition with PAMY as key step, and subsequent condensation with hydrazine. Furthermore, we broadened the variety of dipolarophiles for cycloaddition with PAMY and showed 1,4-diphenylbut-2-yne-1,4-dione **2** as versatile dipolarophile. Besides the verification with NMR spectroscopy and mass spectrometry, the structure of *tert*-butyl substituted **PP-2** was unambiguously confirmed by X-ray single crystal analysis. The investigations of the optoelectronic properties were performed via UV-Vis absorption, fluorescence emission spectroscopy and cyclic voltammetry. Density functional theory (DFT) calculations indicated an intramolecular push-pull behavior caused by the ullazine unit as donor and the pyridazine core as acceptor. Moreover, the pronounced oxidation behavior allowed the formation of the radical cation species of **PP-2** as probed by *in situ* EPR/UV-Vis-NIR spectroelectrochemistry.

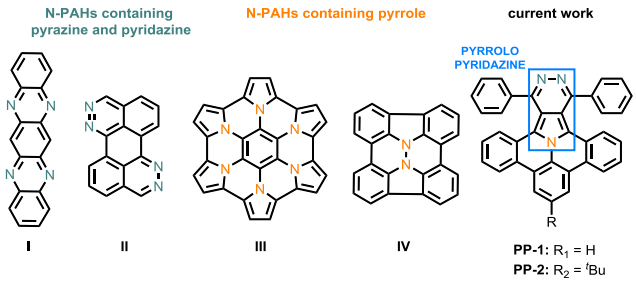

Figure 1. Several examples of N-PAHs (**I-IV**) in comparison to **PP-1** and **PP-**

[a] M. Richter, Y. Fu, Dr. R. Berger, Dr. J. Liu, Prof. Dr. X. Feng
Dresden University of Technology, Center for Advancing Electronics Dresden (cfaed), Faculty of Chemistry and Food Chemistry,
Institute for Molecular Functional Materials
Mommsenstraße 4, 01069 Dresden, Germany
E-mail: xinliang.feng@tu-dresden.de
[b] Dr. E. Dmitrieva, Dr. A. Popov
Leibniz Institute for Solid State and Materials Research, Nanoscale Chemistry
Center of Spectroelectrochemistry
Helmholtzstrasse 20, 01069 Dresden, Germany
[c] Prof. Dr. J. J. Weigand
Dresden University of Technology, Faculty of Chemistry and Food Chemistry
Institute for Inorganic Molecular Chemistry
Mommsenstraße 4, 01069 Dresden, Germany

Supporting information for this article is given via a link at the end of the document.((Please delete this text if not appropriate))

2. For better visualization, the substituents of **I-IV** are obscured.

The targeted compounds **PP-1** and **PP-2** were synthesized in two steps starting from 8*H*-isoquinolino[4,3,2-*de*]phenanthridinium tetrafluoroborate (**1a**) and 2-(*tert*-butyl)-8*H*-isoquinolino[4,3,2-*de*]phenanthridinium tetrafluoroborate (**1b**), respectively (see Scheme 1).[7-8] Intermediates benzo[7,8]indolizino[6,5,4,3-*def*]phenanthridine-1,2-diyl)bis(phenylmethanone) (**3a**) and (8-(tert-butyl)benzo[7,8]indolizino[6,5,4,3-*def*]phenanthridine-1,2-diyl)bis(phenylmethanone) (**3b**) were obtained via 1,3-dipolar cycloaddition of PAMY, which was generated by the addition triethylamine (TEA) from the iminium salts **1a** and **1b**, respectively, and 1,4-diphenylbut-2-yne-1,4-dione (**2**) as dipolarophile with subsequent dehydrogenation using 2,3-dichloro-5,6-dicyano-1,4-benzoquinone (DDQ). After this one pot synthesis, the ketone compounds **3a** and **3b** were obtained in 88% and 86% yield, respectively. The following condensation with hydrazine and purification via methanol precipitation gave the final compounds 1,4-diphenylbenzo[7,8]pyridazino[4',5':1,2]indolizino[6,5,4,3-*def*]phenanthridine (**PP-1**) and 10-(*tert*-butyl)-1,4-diphenylbenzo[7,8]pyridazino[4',5':1,2]indolizino[6,5,4,3-*def*]phenanthridine (**PP-2**) as yellow solids in 66% and 83% yield, respectively. All intermediates and target compounds were fully characterized by high-resolution (HR) atmospheric pressure chemical ionization (APCI) or HR electrospray ionization (ESI) mass spectrometry as well as NMR spectroscopy.

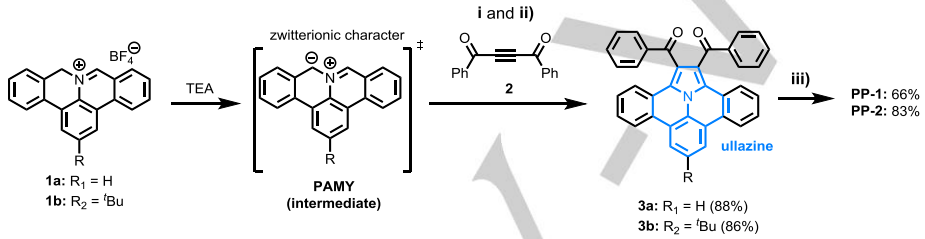

Scheme 1. Synthetic route towards **PP-1** and **PP-2**. Reagents and conditions: i) 1,4-diphenylbut-2-yne-1,4-dione, DCM, 5 min, r.t. ii) DDQ, toluene, r.t., 3h. iii) hydrazine, ethanol, overnight, 80 °C.

The single crystal of **PP-2** was obtained by slow diffusion of methanol into a diethyl ether solution of **PP-2**. The structure of **PP-2** was unambiguously determined by X-ray single-crystal diffraction analysis (Figure 2). The single crystal of **PP-2** showed a planar ullazine motif and a twisted pyridazine ring in an angle of 121° as well as twisted phenyl substituents in an angle of 52° (Figure 2a). In the pyridazine unit, the lengths of the N-N (A) and C-N (B) bonds are 1.36 Å and 1.32 Å, respectively (Figure 2b). Moreover, in the pyrrole core,C-N (F) bond length is 1.39 Å and the C-C bond lengths are 1.41 and 1.43 Å, respectively (Figure 2b). The bond lengths of the pyrrole and pyridazine motifs are in agreement with the literature values.[4c, 7, 9a] Crystals of **PP-2** are arranged in a brick-wall fashion with π-π distance of 3.40 Å between neighboring molecules (Figure 2c).

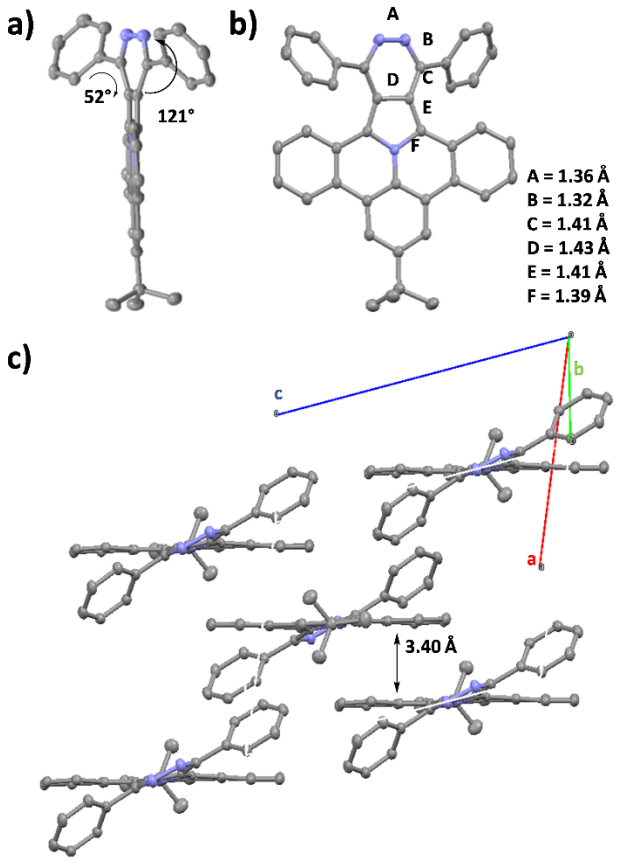

Figure 2. (a) Side view of the single crystal structure of **PP-2**. (b) Top view of the single crystal structure of **PP-2**. (c) The crystal packing of **PP-2**.

The optical properties of **PP-1** and **PP-2** were investigated by solvent-dependent UV-Vis absorption and fluorescence emission spectroscopy in acetonitrile (ACN), dichloromethane (DCM), diethy lether (Et_2O) and toluene. In the UV-Vis absorption as well as fluorescence emission spectra, there is no difference between **PP-1** and **PP-2**, which confirmed that the *tert*-butyl substituent does not apparently influence the optoelectronic properties (see SI). As a typical example, the solvent-dependent UV-Vis absorption spectra of **PP-2** are shown in Figure 3a. The solutions of **PP-2** in toluene and Et_2O exhibit an intensive broad absorption band between 400 and 500 nm with absorption maxima ($\lambda_{max,\ abs}$) at 433 nm and 428 nm, respectively. In more polar solvents such as ACN and DCM, the absorption spectra are better resolved and the $\lambda_{max,\ abs}$ of **PP-2** revealed a hypsochromic shift up to 14 nm in ACN. The optical energy gap (ΔE_g^{opt}) of **PP-2** calculated from the absorption maximum of UV-Vis absorption spectrum in DCM is 2.93 eV. In contrast, the emission maximum ($\lambda_{max,\ ems}$) of **PP-2** is observed at 560 nm showed no solvent-dependency (see SI). The fluorescence quantum yield (Φ) determined for **PP-2** is Φ = 0.22 in DCM (see SI).[10] The electrochemical properties of **PP-2** were further investigated by cyclic voltammetry (CV) which allowed the determination of the energy levels of the frontier orbitals. In DCM, **PP-2** showed a reversible oxidation wave (0.5 V vs Fc^+/Fc), which becomes irreversible if further redox processes occur (see Figure 3b). Additional, two further overlapping oxidation waves were detected (Figure 3b). A reduction behavior was not observed in the available potential window (see SI). Thus the highest occupied molecular orbital (HOMO) was estimated based on the half-wave potential of the first reversible oxidation to be -5.30 eV. The lowest unoccupied molecular orbital (LUMO), which was deduced by the optical band gap and electrochemical HOMO level, is -2.37 eV. All calculated optoelectronic data of **PP-1** and **PP-2** are summarized in the SI.

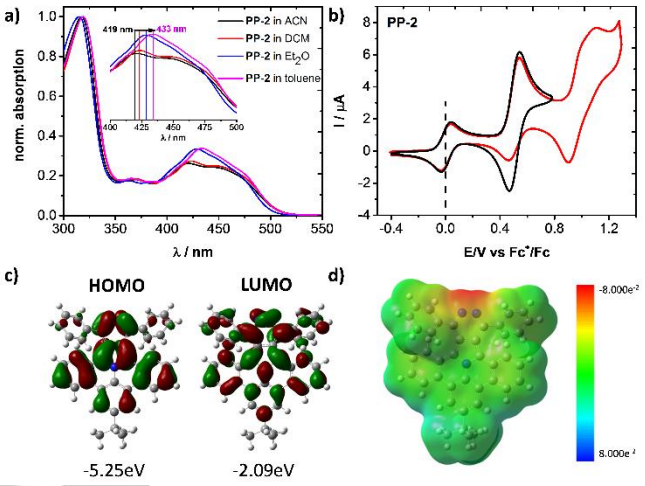

Figure 3. (a) Solvent-dependent UV-Vis absorption spectra of **PP-2** in acetonitrile (ACN), dichloromethane (DCM), diethyl ether (Et_2O) and toluene. Inset: zoom of the solvent-dependent UV-Vis absorption spectra of **PP-2** from 400 to 500 nm. (b) Cyclic voltammogram of **PP-2** recorded in DCM with 0.1 M *n*-Bu_4NPF_6 as a supporting electrolyte at 100 mVs^{-1} from -0.4 V to 0.8 V (black line) and -0.4 V to 1.3 V (red line). AgCl-coated Ag-wire was used as a reference electrode, platinum as a working electrode and Pt-wire as a counter electrode. (c) Calculated molecular orbitals and energy level of **PP-2** with a B3PW91 functional and 6-31G*basis set (HOMO level: left; LUMO level: right). (d) ESP calculation of **PP-2** (red: negative charge distribution and blue: positive charge distribution).

The electronic ground states of **PP-1** and **PP-2** were investigated by density functional theory (DFT) with a Gaussian 09 package. The geometry of **PP-1** and **PP-2** was optimized by the B3PW91/6-31G* based on the single crystal structure. The graphical representations of the HOMO and the LUMO are presented in Figure 3c exemplified for **PP-2**. The HOMO mainly distributed at the dibenzoullazine motif and partially at the pyridazine core as well as phenyl substituents (see SI). In contrast, the LUMO equally delocalized over the full π-system. The calculated HOMO levels (**PP-1**: -5.28 eV; **PP-2**: -5.25 eV) are in agreement with the experimental derived value (**PP-2**: -5.30 eV) from CV measurements. Furthermore, the calculated energy gaps (**PP-1**: 3.17 eV; **PP-2**: 3.16 eV) are in accordance with the optical energy gap (2.93 eV). For a deeper insight into the electronic nature, electronic static potential (ESP) were investigated (**PP-1**: SI and **PP-2:** Figure 3d). **PP-2** revealed a neutral charge distribution over the whole structure (green color). Negative charge distribution (red color) was found in the pyridazine unit which can be explained by the localization of the

lone pairs of electrons and the higher electronegativity of the nitrogen atoms. The structure with a pyridazine core as acceptor and the ullazine unit as donor explains the push-pull behavior.[11] Furthermore, anisotropy of the induced current density (ACID) calculations were performed to verify the aromatic features and confirmed the global aromaticity of the **PP-1** and **PP-2** (see SI).

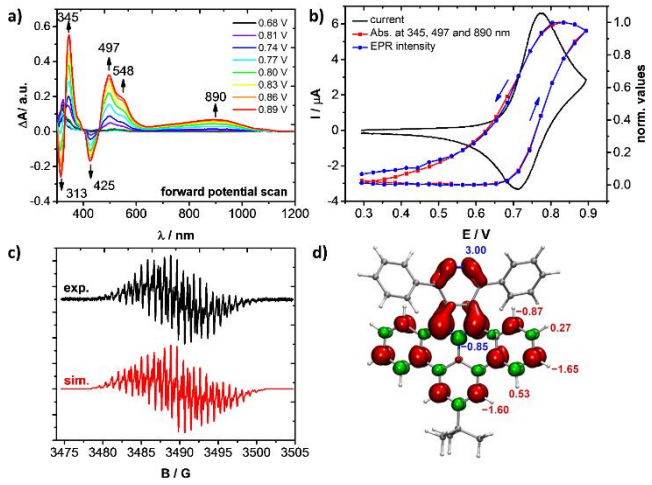

Figure 4. In situ EPR/UV-Vis-NIR spectroelectrochemical measurement of **PP-2**. (a) UV-Vis-NIR absorption spectra measured during the electrochemical oxidation of **PP-2**. (b) Black: cyclic voltammogram of the oxidation (0.1 M *n*-Bu_4NPF_6 in DCM, scan rate = 5 mVs^{-1}). Red: potential dependence of UV-Vis-NIR absorption bands (λ = 345, 497 and 890 nm). Blue: potential dependence of double integrated EPR intensity. (c) Experimental and simulated EPR spectra of **PP-2$^{\bullet+}$**. (d) DFT-computed spin density distribution in the radical cation **PP-2$^{\bullet+}$** along with hyperfine coupling constants obtained from the fit of experimental EPR spectrum (the sign and the values are assigned to different types of atoms based on B3LYP functional with EPR-III basis set for N and H atoms, and TZVP basis set for carbons, Orca package[12]; *a*(^{14}N) constants are shown in dark blue, *a*(^{1}H) constants - in red).

The protonation of **PP-1** and **PP-2** with triflic acid (TfOH) was performed and monitored via NMR spectroscopy, HR matrix-assisted laser desorption/ionization (MALDI) time of flight (ToF) MS and UV-Vis absorption titration (see SI). Furthermore, *in situ* electron paramagnetic resonance (EPR) and UV-Vis-near-infrared (NIR) absorption spectroscopy enable the detailed investigation of the radical species of **PP-2**. The spectroelectrochemical results of **PP-2** are displayed in Figure 4. Upon the oxidation, UV-Vis-NIR absorption spectra manifest new absorption maxima at 345, 497, 548 and 890 nm (Figure 4a). The potential profiles of the absorption bands and the EPR intensity are identical (Figure 4b). Thus, the emerging absorption bands can be obviously attributed to the radical cation **PP-2$^{\bullet+}$**. EPR spectrum of radical cation **PP-2$^{\bullet+}$** shows a well resolved hyperfine structure due to the interaction of the unpaired electron spin with nuclei spins of nitrogen and protons (Figure 4c). DFT calculations demonstrate that the spin density is delocalized over the whole framework and no spin density is delocalized at the phenyl-substituents. The largest coupling constants are predicted for the N-N bond and for protons at the perimeter of the PAH. For a more precise interpretation of the hyperfine pattern, the spectrum is fitted using EasySpin software[13] and DFT-derived hyperfine[12] coupling constant as starting values. Perfect match to the experimental data is obtained for 2×*a*(^{14}N) of 3.00 G, the internal nitrogen with a constant of −0.85 G, and five couples of protons with *a*(^{1}H) constants of −1.65, −1.60, −0.87, 0.83, and 0.27 G (Figure 4d). Comparable hfc constant for all protons on the perimeter of the PAH core as well as considerable hfc values for nitrogen atoms prove delocalization of the spin density in radical cation (and hence also the HOMO in the pristine **PP-2**) over the whole aromatic moiety.

In summary, we have demonstrated an efficient two-step synthesis of the first diphenyl-substituted pyrrolopyridazine-core-embedded N-PAHs via one-pot 1,3-dipolar cycloaddition and dehydrogenation as well as subsequent condensation with hydrazine. The chemical identities were elucidated by NMR spectroscopy, MS and X-ray single crystal analysis for **PP-2**, which revealed a twisted pyridazine ring with a N-N bond length of 1.36 Å. An intramolecular push-pull behavior between the ullazine as donor and the pyridazine core as acceptor unit within **PP-1** and **PP-2** was confirmed by DFT calculations. Furthermore, *in situ* EPR/UV-Vis-NIR spectroelectrochemistry showed the formation of radical cation species **PP-2$^{\bullet+}$** with broad NIR absorption maximum at 890 nm. **PP-1** and **PP-2** could be material candidates for organic field effect transistor (OFET) applications or chemical/bio sensing.

Experimental Section

The synthesis and the analytical data of 8*H*-isoquinolino[4,3,2-*de*]phenanthridinium tetrafluoroborate (**1a**) and 2-(*tert*-butyl)-8*H*-isoquinolino[4,3,2-*de*]phenanthridinium tetrafluoroborate (**1b**) were reported in our previous work.[7-8]

General procedure for the synthesis of the intermediates (3a and 3b)

In a dry and inert Schlenk tube the iminium salt (1.00 eq.) and 1,4-diphenyl-2-butyne-1,4-dione (**2**, 173 mg, 739 µmol, 1.20 eq.) were dissolved in anhydrous dichloromethane (DCM, 20 ml). Anhydrous triethylamine (7.4 mmol, ~12.00 eq) was added under stirring in one portion. The reaction was stirred for several minutes and transferred to a round-bottom flask afterwards. Solvents and residual triethylamine were removed under reduced pressure to obtain the crude product. 2,3-Dichloro-5,6-dicyano-1,4-benzoquinone (DDQ, 559 mg, 2.47 mmol, 4.00 eq.) was added and the flask was sealed with a septum as well as purged with argon for five minutes. Anhydrous toluene (20 ml) was added via syringe. After 30 minutes, the reaction was quenched by addition of water (10 ml) and extracted with DCM (20 ml) five times. The combined organic layers were washed with brine and dried over magnesium sulfate. The solvent was removed under reduced pressure. The residue was dissolved in a minimum amount of DCM (10 ml) and precipitated in methanol (300 ml). The precipitate was filtered.

3a: M_p = 360°C. **^{1}H-NMR (600 MHz, $C_2D_2Cl_4$):** δ = 8.39 (d, *J* = 8.1 Hz, 2H), 8.34 (d, *J* = 8.1 Hz, 2H), 7.95 (dd, *J* = 8.2, 0.6 Hz, 2H), 7.71 (t, *J* = 8.0 Hz, 1H), 7.53 (dd, *J* = 8.2, 1.1 Hz, 4H), 7.49 – 7.45 (m, 2H), 7.42 (dd, *J* = 10.6, 4.2 Hz, 2H), 7.32 – 7.26 (m, 2H), 7.21 (t, *J* = 7.8 Hz, 4H) ppm. **^{13}C-NMR (151 MHz, $C_2D_2Cl_4$):** δ 195.5, 139.2, 133.5, 130.2, 129.1, 129.1, 128.7, 128.4, 127.0, 125.6, 125.5, 124.8, 124.6, 123.4, 121.6,

121.1 ppm. The recorded ^{13}C-NMR spectrum of intermediate **3a** displays 16 detectable peaks, which can be assigned to 9x CH and 7x quarternary carbon atoms, respectively. The peak of one quarternary carbon could not resolve and is obviously overlapping. **HR-MS (APCI-MS):** m/z ([M+H]$^+$) = 500.1642, calcd. for $C_{36}H_{22}NO_2$: m/z = 500.1650; error = -1.6 ppm. **IR:** $\tilde{\nu}$ = 2976, 2903, 1644, 735, 690 cm^{-1}.

3b: M_p = 308°C. **^{1}H-NMR (600 MHz, $C_2D_2Cl_4$):** δ 8.42 (s, 2H), 8.38 (d, *J* = 8.2 Hz, 2H), 7.95 (d, *J* = 8.0 Hz, 2H), 7.53 (dd, *J* = 8.2, 1.0 Hz, 4H), 7.49 – 7.45 (m, 2H), 7.44 – 7.39 (m, 2H), 7.32 – 7.25 (m, 2H), 7.21 (t, *J* = 7.8 Hz, 4H), 1.52 (s, 9H) ppm. **^{13}C-NMR (151 MHz, $C_2D_2Cl_4$):** δ 195.5, 148.4, 139.2, 133.6, 130.1, 128.9, 128.7, 128.3, 127.3, 127.2, 125.7, 124.9, 124.5, 123.3, 122.9, 121.0, 118.6, 35.67, 32.1 ppm. **HR-MS (APCI-MS):** m/z ([M+H]$^+$) = 556.2262, calcd. for $C_{40}H_{30}NO_2$: m/z = 556.2276; error = -2.5 ppm. **IR:** $\tilde{\nu}$ = 2957, 1641, 753, 695 cm^{-1}.

General procedure for the synthesis of N-PAHs with Pyrrolopyridazine Core (PP-1 and PP-2)

In a dry and inert 50 ml Schlenk flask, intermediate (**3a** or **3b**, 1.00eq.) and an excess of hydrazine monohydrate (~5.00 eq.) was suspended in anhydrous ethanol (20 ml). Afterwards, stirring was continued overnight at 78 °C. After cooling down to room temperature, the reaction mixture was quenched with water and extracted with DCM (20 ml) five times. The combined organic layers were washed with brine and dried over magnesium sulfate. The solvent was removed under reduced pressure and the residue was dissolved in a minimum amount of DCM (~10 ml) and precipitated in methanol (300 ml) to obtain the target compounds as solids.

PP-1: M_p = 427 °C. **^{1}H-NMR (600 MHz, $C_2D_2Cl_4$):** δ 8.50 (d, *J* = 8.0 Hz, 2H), 8.35 (d, *J* = 8.1 Hz, 2H), 7.85 (t, *J* = 7.9 Hz, 1H), 7.80 – 7.70 (m, 4H), 7.48 (t, *J* = 7.4 Hz, 2H), 7.42 (t, *J* = 7.4 Hz, 4H), 7.39 (dd, *J* = 11.2, 3.9 Hz, 2H), 7.21 (d, *J* = 8.0 Hz, 2H), 7.00 (t, *J* = 7.6 Hz, 2H) ppm. **^{13}C-NMR (151 MHz, $C_2D_2Cl_4$):** δ 153.5, 139.4, 129.9, 129.2, 129.0, 128.1, 127.4, 126.4, 125.4, 124.5, 122.9, 121.2, 119.4 ppm. Due to the low solubility in $C_2D_2Cl_4$ chemical shifts of 13-C nuclei were derived from the HMBC experiment. Unfortunately, not all carbon atoms could be detected. **HR-MS (APCI-MS):** m/z ([M+H]$^+$) = 496.1802, calcd. for $C_{36}H_{22}N_3$: m/z = 496.1813; error = -1.8 ppm. **IR:** $\tilde{\nu}$ = 2979, 2909, 755, 695 cm^{-1}.

PP-2: M_p = 403 °C. **^{1}H-NMR (600 MHz, $C_2D_2Cl_4$):** δ 8.52 (s, 2H), 8.39 (d, *J* = 8.1 Hz, 2H), 7.85 – 7.66 (m, 4H), 7.50 – 7.45 (m, 2H), 7.40 (ddd, *J* = 15.4, 11.5, 4.4 Hz, 6H), 7.21 – 7.17 (m, 2H), 7.01 – 6.97 (m, 2H), 1.53 (s, 9H) ppm. **^{13}C-NMR (151 MHz, $C_2D_2Cl_4$):** δ 153.6, 150.1, 139.5, 130.0, 129.8, 129.2, 129.1, 128.0, 127.5, 127.3, 126.7, 125.0, 124.7, 122.7, 119.2, 118.4, 112.4, 35.8, 32.0 ppm. **HR-MS (ESI-MS):** m/z ([M+H]$^+$) = 552.2435, calcd. for $C_{40}H_{30}N_3$: m/z = 552.2439; error = - 0.72 ppm. **IR:** $\tilde{\nu}$ = 2961, 2908, 758, 692 cm^{-1}.

General procedure for the protonation of PP-1 and PP-2 with triflic acid (TfOH)

In a NMR tube, a triflic acid (1.0 eq.) was added to a solution of **PP-1** and **PP-2** in $C_2D_2Cl_4$. After the addition of TfOH and short mixing for two minutes, an unblemished colour change from yellow to red was observed. The reaction was carried out under ambient conditions. The NMR spectrum showed a shift of the signals. The corresponding HR-MALDI-ToF confirmed the protonation and showed no decomposition.

PP-1+H$^+$: ^{1}H-NMR (300 MHz, $C_2D_2Cl_4$): δ 8.58 (d, J = 8.1 Hz, 2H), 8.42 (d, J = 8.3 Hz, 2H), 7.95 (t, J = 8.2 Hz, 1H), 7.75 (d, J = 7.0 Hz, 4H), 7.63 – 7.36 (m, 8H), 7.15 (d, J = 8.0 Hz, 2H), 7.03 (t, J = 7.7 Hz, 2H) ppm. **^{13}C-NMR (75 MHz, $C_2D_2Cl_4$):** δ 154.5, 130.1, 129.8, 128.5, 127.3, 125.6, 123.47, 123.3, 122.3, 122.0 ppm. Unfortunately, not all carbon atoms could be detected due to the low solubility. **HR-MS (MALDI-ToF):** m/z ([M+H]$^+$) = 496.1876, calcd. for $C_{36}H_{22}N_3$: m/z = 496.1813; error = 12.69 ppm.

PP-2+H$^+$: ^{1}H-NMR (300 MHz, $C_2D_2Cl_4$): δ 8.64 (s, 2H), 8.49 (d, J = 8.2 Hz, 2H), 7.76 (d, J = 7.5 Hz, 4H), 7.67 – 7.41 (m, 8H), 7.08 (dt, J = 15.2, 7.8 Hz, 4H), 1.56 (s, 9H). **^{13}C-NMR (75 MHz, $C_2D_2Cl_4$):** δ 154.5, 133.4, 131.9, 129.8, 129.6, 127.9, 126.4, 122.8, 118.6, 33.3, 31.6 ppm. Due to the low solubility in $C_2D_2Cl_4$ chemical shifts of 13-C nuclei were derived from the HMBC experiment. Unfortunately, not all carbon atoms could be detected. **HR-MS (MALDI-ToF):** m/z ([M+H]+) = 552.2429, calcd. for $C_{40}H_{30}N_3$: m/z = 552.2439; error = - 1.81 ppm.

CCDC 1889654 (**PP-2**) contain the supplementary crystallographic data for this paper. This data can be obtained free of charge from The Cambridge Crystallographic Data Centre.

Acknowledgements

We thank the European Union's Horizon 2020 research and innovation program under grant agreement No 696656 (Graphene Flagship Core2), the German Research Foundation (DFG) within the Cluster of Excellence "Center for Advancing Electronics Dresden (cfaed)" and EnhanceNano (No. 391979941) as well as the European Social Fund and the Federal State of Saxony (ESF-Project "GRAPHD", TU Dresden) for financial support. Furthermore, we thank F. Drescher, Dr. S. Machill, Prof. E. Brunner and Dr. T. Lübken for HR-MS measurements and NMR measurements, respectively, and Ulrike Nitzsche for the help with computational resources at IFW Dresden. We thank the Center for Information Services and High Performance Computing (ZIH) at TU Dresden for generous allocations of compute resources.

Keywords: azomethine ylide • cycloaddition • heterocycles • polycyclic aromatic hydrocarbons • radical cations •

[1] a)M. Ball, Y. Zhong, Y. Wu, C. Schenck, F. Ng, M. Steigerwald, S. Xiao, C. Nuckolls, *Acc. Chem. Res.* **2015**, *48*, 267-276; b)X. Yan, L.-s. Li, *J. Mater. Chem.* **2011**, *21*, 3295-3300; c)K. K. Baldridge, J. S. Siegel, *Angew. Chem. Int. Ed.* **2013**, *52*, 5436-5438; d)W. Pisula, X. Feng, K. Müllen, *Chem. Mater.* **2011**, *23*, 554-567; e)Y. Morita, S. Suzuki, K. Sato, T. Takui, *Nat. Chem.* **2011**, *3*, 197; f)Z. Sun, Q. Ye, C. Chi, J. Wu, *Chem. Soc. Rev.* **2012**, *41*, 7857-7889; g)W. Chen, X. Li, G. Long, Y. Li, R. Ganguly, M. Zhang, N. Aratani, H. Yamada, M. Liu, Q. Zhang, *Angew. Chem. In. Ed.* **2018**, *57*, 13555-13559; h)W. Chen, X. Li, G. Long, Y. Li, R. Ganguly, M. Zhang, N. Aratani, H. Yamada, M. Liu, Q. Zhang, *Angew. Chem.* **2018**, *130*, 13743-13747; i) J. Li, S. Chen, Z. Wang, Q. Zhang, *Chem. Rec.* **2016**, *16*, 1518-1530.

[2] a)R. Rieger, K. Müllen, *J. Phys. Org. Chem.* **2010**, *23*, 315-325; b)A. Narita, X.-Y. Wang, X. Feng, K. Müllen, *Chem. Soc. Rev.* **2015**, *44*, 6616-6643; c)Z. Sun, J. Wu, *J. Mater. Chem.* **2012**, *22*, 4151-4160; d)K. Kawasumi, Q. Zhang, Y. Segawa, L. T. Scott, K. Itami, *Nat. Chem.* **2013**, *5*, 739; e)P.-Y. Gu, Y. Zhao, J.-H. He, J. Zhang, C. Wang, Q.-F. Xu, J.-M. Lu, X. W. Sun, Q. Zhang, *J. Org. Chem.* **2015**, *80*, 3030-3035; f)P.-Y. Gu, Z. Wang, G. Liu, H. Yao, Z. Wang, Y. Li, J. Zhu, S. Li, Q. Zhang, *Chem. Mater.* **2017**, *29*, 4172-4175.

[3] a)J. Cai, C. A. Pignedoli, L. Talirz, P. Ruffieux, H. Söde, L. Liang, V. Meunier, R. Berger, R. Li, X. Feng, K. Müllen, R. Fasel, *Nat. Nanotechnol.* **2014**, *9*, 896; b)H. Sahabudeen, H. Qi, B. A. Glatz, D. Tranca, R. Dong, Y. Hou, T. Zhang, C. Kuttner, T. Lehnert, G. Seifert, U. Kaiser, A. Fery, Z. Zheng, X. Feng, *Nat. Commun.*

2016, *7*, 13461; c)L. Ji, A. Friedrich, I. Krummenacher, A. Eichhorn, H. Braunschweig, M. Moos, S. Hahn, F. L. Geyer, O. Tverskoy, J. Han, C. Lambert, A. Dreuw, T. B. Marder, U. H. F. Bunz, *J. Amer. Chem. Soc.* **2017**, *139*, 15968-15976; d)M. Richter, K. S. Schellhammer, P. Machata, G. Cuniberti, A. Popov, F. Ortmann, R. Berger, K. Müllen, X. Feng, *Org. Chem. Front.* **2017**, *4*, 847-852; e)M. Gsänger, J. H. Oh, M. Könemann, H. W. Höffken, A.-M. Krause, Z. Bao, F. Würthner, *Angew. Chem. Int. Ed.* **2010**, *49*, 740-743; f)M. Gsänger, J. H. Oh, M. Könemann, H. W. Höffken, A.-M. Krause, Z. Bao, F. Würthner, *Angew. Chem.* **2010**, *122*, 752-755; g)A. Mateo-Alonso, *Chem. Soc. Rev.* **2014**, *43*, 6311-6324; h)A. Hirsch, B. Nuber, *Acc. Chem. Res.* **1999**, *32*, 795-804; i)Z. Wang, P. Gu, G. Liu, H. Yao, Y. Wu, Y. Li, G. Rakesh, J. Zhu, H. Fu, Q. Zhang, *Chem. Commun.* **2017**, *53*, 7772-7775.

[4] a)U. H. F. Bunz, *Acc. Chem. Res.* **2015**, *48*, 1676-1686; b)U. H. F. Bunz, J. U. Engelhart, *Chem. – Eur. J.* **2016**, *22*, 4680-4689; c)R. Tang, F. Zhang, Y. Fu, Q. Xu, X. Wang, X. Zhuang, D. Wu, A. Giannakopoulos, D. Beljonne, X. Feng, *Org. Lett.* **2014**, *16*, 4726-4729.

[5] a)M. Takase, T. Narita, W. Fujita, M. S. Asano, T. Nishinaga, H. Benten, K. Yoza, K. Müllen, *J. Amer. Chem. Soc.* **2013**, *135*, 8031-8040; b)S. Higashibayashi, P. Pandit, R. Haruki, S.-i. Adachi, R. Kumai, *Angew. Chem. Int. Ed.* **2016**, *55*, 10830-10834; c)S. Higashibayashi, P. Pandit, R. Haruki, S.-i. Adachi, R. Kumai, *Angew. Chem.* **2016**, *128*, 10988-10992.

[6] a)H. Wang, T. Maiyalagan, X. Wang, *ACS Catal.* **2012**, *2*, 781-794; b)D. Wei, Y. Liu, *Adv. Mater.* **2010**, *22*, 3225-3241.

[7] R. Berger, M. Wagner, X. Feng, K. Müllen, *Chem.Sci.* **2015**, *6*, 436-441.

[8] a)X.-Y. Wang, M. Richter, Y. He, J. Björk, A. Riss, R. Rajesh, M. Garnica, F. Hennersdorf, J. J. Weigand, A. Narita, R. Berger, X. Feng, W. Auwärter, J. V. Barth, C.-A. Palma, K. Müllen, *Nat. Commun.* **2017**, *8*, 1948; b)S. Ito, Y. Tokimaru, K. Nozaki, *Chem. Commun.* **2015**, *51*, 221-224.

[9] a)M. Richter, S. Hahn, E. Dmitrieva, F. Rominger, A. Popov, U. H. F. Bunz, X. Feng, R. Berger, *Chem. – Eur. J.* **2019**, *25*, 1345-1352; b)Y. Tokimaru, S. Ito, K. Nozaki, *Angew. Chem. Int. Ed.* **2017**, *56*, 15560-15564; c)Y. Tokimaru, S. Ito, K. Nozaki, *Angew. Chem.* **2017**, *129*, 15766-15770; d)Y. Tokimaru, S. Ito, K. Nozaki, *Angew. Chem. Int. Ed.* **2018**, *57*, 9818-9822; e)Y. Tokimaru, S. Ito, K. Nozaki, *Angew. Chem.* **2018**, *130*, 9966-9970.

[10] G. A. Crosby, J. N. Demas, *J. Phys. Chem.* **1971**, *75*, 991-1024.

[11] B. König, *Angew. Chem.* **1996**, *108*, 115-116.

[12] F. Neese, *WIREs Comput. Mol. Sci.* **2012**, *2*, 73-78.

[13] S. Stoll, A. Schweiger, *J. Magn. Res.* **2006**, *178*, 42-55.

Entry for the Table of Contents (Please choose one layout)

COMMUNICATION

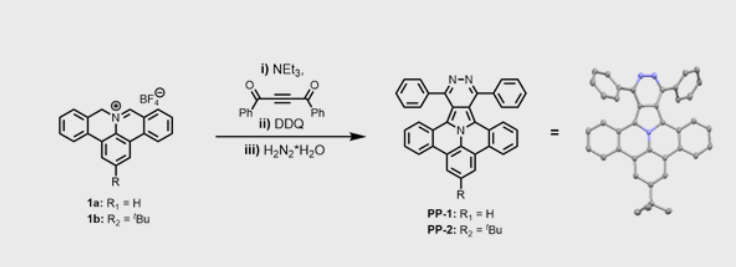

*M. Richter, Y. Fu, E. Dmitrieva, J. J. Weigand, A. Popov, R. Berger, J. Liu, X. Feng **

Page No. – Page No.

A Polycyclic Aromatic Hydrocarbon Containing A Pyrrolopyridazine Core

Polycyclic aromatic hydrocarbons (PAHs) with a pyrrolopyridazine (**PP-1** and **PP-2**) core have been synthesized by 1,3-cycloaddition of polycyclic aromatic azomethine ylides (PAMYs) and 1,4-diphenylbut-2-yne-1,4-dione as dipolarophile as well as subsequent condensation reaction with hydrazine. The properties were investigated by single-crystal X-ray analysis, UV-Vis absorption spectroscopy, cyclic voltammetry and computational modeling. Furthermore, the radical cation species of the *tert*-butyl-substituted **PP-2** was obtained by EPR/UV-Vis-NIR spectroelectrochemistry.